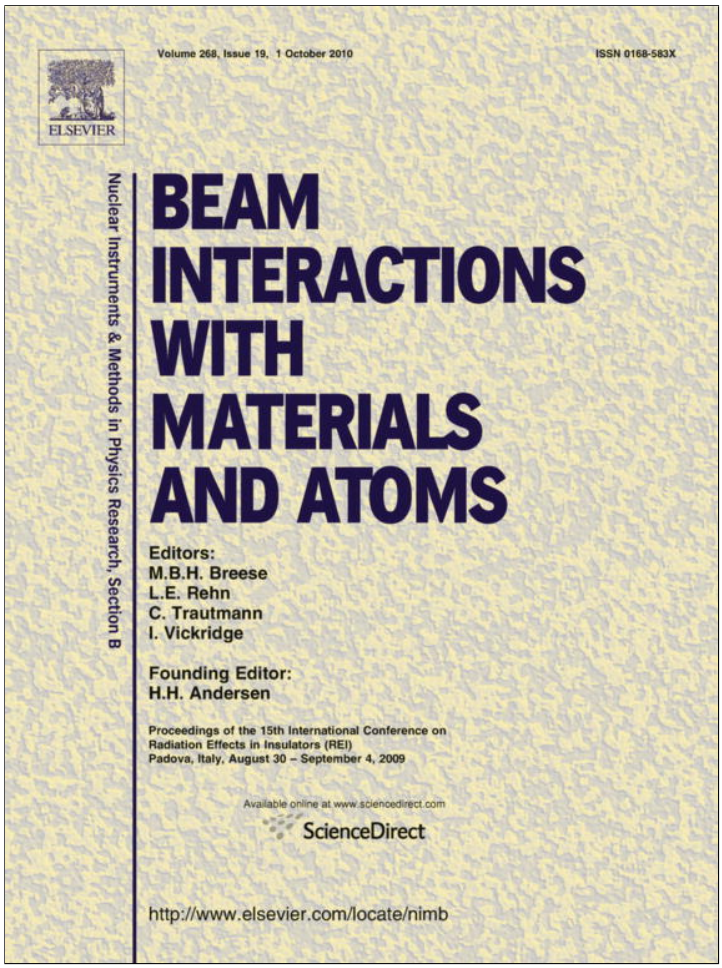

Nuclear Instruments and Methods in Physics Research B 268 (2010) 3055–3058

Contents lists available at ScienceDirect

Nuclear Instruments and Methods in Physics Research B

journal homepage: www.elsevier.com/locate/nimb

Void superlattice formation in electron irradiated CaF_2: Theoretical analysis

V.N. Kuzovkov [a], E.A. Kotomin [a,*], P. Merzlyakov [a], G. Zvejnieks [a], K.D. Li [b,c], T.H. Ding [b,c], L.M. Wang [b,c]

[a] Institute for Solid State Physics, University of Latvia, 8 Kengaraga, LV 1063 Riga, Latvia
[b] Department of Materials Science and Engineering, University of Michigan, Ann Arbor, MI 48109, USA
[c] Department of Nuclear Engineering and Radiological Sciences, University of Michigan, Ann Arbor, MI 48109, USA

ARTICLE INFO

Article history:
Received 24 September 2009
Received in revised form 20 April 2010
Available online 8 May 2010

Keywords:
Electron irradiation
Kinetic Monte Carlo
Void superlattice
Computer modeling
CaF_2

ABSTRACT

CaF_2 is widely adopted as deep-UV window material and thin film optical coating. The void superlattice was observed experimentally under electron irradiation at room temperature. We performed kinetic Monte Carlo (kMC) simulations of the initial stages of the process when short- and intermediate-range order of defects in small Ca colloids and larger interstitial aggregates (F_2 gas voids) is created. The kMC model includes fluorine interstitial–vacancy pair creation, defect diffusion, similar defect attraction and dissimilar defect recombination. Special attention is paid to the statistical analysis of the defect aggregate distribution functions under different conditions (dose rate, defect migration and recombination rates). These simulations demonstrate that under certain conditions the dissimilar aggregate recombination is strongly suppressed which stimulates growth of mobile interstitial aggregates that is a precondition for further void ordering into a superlattice.

1. Introduction

As is well known, irradiation of many metallic and insulating solids with energetic particles, such as heavy ions, neutrons, electrons, can result in a formation of *ordered structures* including periodic defect walls, bubble lattices, void lattices and periodic compositions in alloys [1,2]. The particular ordered structures arising in such *open dissipative systems far from equilibrium* depend on a type, energy, and flux of the energetic particles as well on the temperature. It was noticed [3] that despite the difference in the appearance, a similar underlying mechanism may be invoked to explain the *self-organization behavior* of these structures. In particular, it was observed in situ TEM [4] that under electron beam (200 keV) irradiation of insulating CaF_2 at room temperature primary radiation defects create clusters which transforms under certain radiation dose into void superlattice. Experimental data [5] support the conclusion that these are F_2 gas voids formed by aggregation of fluorine interstitials rather Ca colloids as was generally accepted earlier.

In this paper, we performed kinetic Monte Carlo (kMC) modeling of the initial stage of such a superlattice formation with the focus on the kinetics of similar defect clustering, defect spatial distribution and void formation.

2. Experimental data analysis

Experimental information usually is obtained in a form of TEM images (Fig. 1(a)). We have created a filter that average the spatial snapshot color intensities using the Gaussian function. The dark color extremum regions are then associated with void clusters (Fig. 1(b)).

This procedure allows us to obtain the void cluster size and thus the cluster distribution, N_s, as a function of the numbers of atoms therein. In a general case, the cluster density depends on the average cluster size, $\langle s\rangle$, accumulated total defect concentration C as well as other system and irradiation parameters.

The standard method to analyze the dynamics of cluster distribution is based on the dynamical scaling ([6] and references therein). Using a few universal parameters, we calculate the function $F(s) = N_s\langle s\rangle^2/C$ characterizing the cluster distribution over the number of defects s therein (Fig. 1(c)) for the experimental filtered image (Fig. 1(b)). This distribution demonstrates the characteristic cluster size of $\langle s\rangle = 45$ atoms (considering an image as a 2D [1 0 0] plane).

When the scaling assumption holds, the universal scaling function $\widetilde{F}$ exist such that $F(s/\langle s\rangle) \to \widetilde{F}(s/\langle s\rangle)$. This function depends on a single dimensionless parameter $u = s/\langle s\rangle$, where the normalization condition $\int_0^\infty \widetilde{F}(u)\mathrm{d}u = \int_0^\infty \widetilde{F}(u)u\,\mathrm{d}u = 1$ holds [6]. An existence of the scaling function means a self similarity in a system at different scales.

The statistical analysis could be accompanied with the calculation of the *distinctive spatial scale* ξ (average distance between

* Corresponding author.
E-mail address: kotomin@latnet.lv (E.A. Kotomin).

0168-583X/$ - see front matter © 2010 Elsevier B.V. All rights reserved.
doi:10.1016/j.nimb.2010.05.040

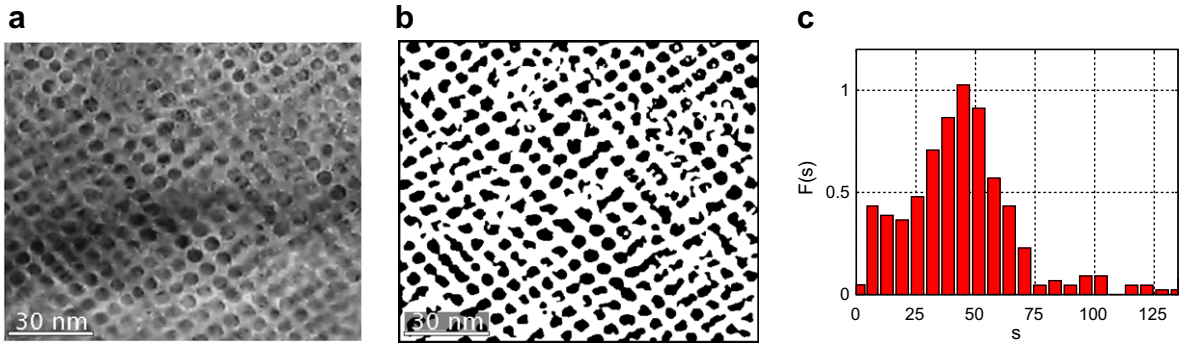

Fig. 1. Over-focused bright-field image of voids in CaF_2 extracted from a digital video recorded during in situ TEM observation (a) and its filtered version (b). The corresponding cluster scaling function (c) with detected parameters: void concentration $C = 0.32$, superlattice size $\xi = 12$ (in the units of lattice constant), average cluster size, $\langle s \rangle = 45$ atoms.

defect clusters [7]). Its simple estimate can be obtained as $\xi = 1/N$, where $N = \sum_s N_s$ is the total cluster density. In the considered example (Fig. 1), we obtain $\xi = 12$ (in the units of CaF_2 lattice constant $a_0 = 5.64$ Å), i.e. 68 Å.

3. Kinetic Monte Carlo simulations

One of the main goals of our kMC modeling is to demonstrate an appearance of stable large interstitial fluorine clusters whose growth dominates over formation of small dimers and other new aggregation germs. This needs reliable statistics for the cluster size (number of defects) distribution.

The KMC simulations were performed using *the standard model* dynamics and *pair algorithm* (for a detailed description, see, e.g. [8]). In calculations we used a discrete square lattice $L \times L$ of size L that is typically around 200 lattice constants a_0. The kinetic model for two kinds of primary radiation defects – fluorine interstitials i and vacancies v – consists of the following steps:

(i) Creation of an uncorrelated defect pair i and v in empty lattice sites with the dose rate p.
(ii) Defect hops into nearest neighbor (NN) empty site with the rate ν_i or ν_v.
(iii) We took into account also the defect annihilation reaction with the rate r between i and v ($i + v = 0$) which are NN.

As a basic model, one can consider the irreversible defect clustering when new defect sticks to the existing cluster as soon as approaches to within a NN distance to its boundary.

Thus our model has four parameters: hopping rates of interstitials, ν_i, and vacancies, ν_v, defect creation rate p (in displacements per atom per second, dpa), and the recombination rate r, respectively. It is convenient to use time units such that $p = 1\ s^{-1}$ and to fix a vacancy hopping frequency, which we have chosen $\nu_v = 0.25 \times 10^6\ s^{-1}$, unless stated otherwise. Computer simulations were performed on the BalticGrid computers [9], where a large number of independent jobs were run simultaneously in order to acquire good statistics of the results.

We have simulated four different cases:

(i) a symmetrical (normal) diffusion ($\nu_i = \nu_v = r$);
(ii) a fast interstitial diffusion and reaction ($\nu_i = r > \nu_v$);
(iii) a fast ($r > \nu_i = \nu_v$) reaction;
(iv) and lastly, slow ($r < \nu_i = \nu_v$) reaction.

As we discussed recently [7], void superlattice formation needs a growth of similar defect clusters of close sizes which are relatively mobile for a further reordering into a superlattice. We analyze below how a choice of diffusion and reaction rate parameters affects the defect cluster growth and its size distribution. For better statistics we averaged the results over a series of kMC simulations with identical parameter sets.

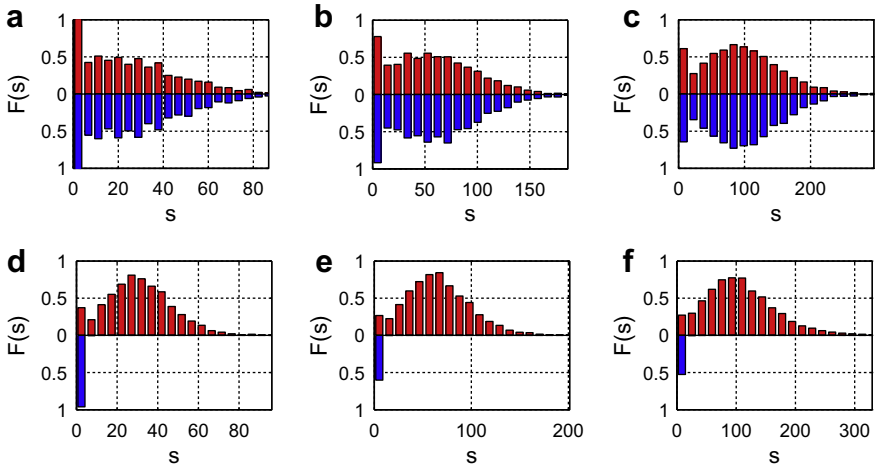

Fig. 2. Cluster distribution dependence on defect concentration, C; s is a number of defects in a cluster. First row (normal diffusion limit (i)), kinetic parameters are: $r = \nu_i = \nu_v$ and C: (a) 0.05, (b) 0.10 and (c) 0.15. Second row (fast interstitial diffusion and reaction (ii)), parameters $r = \nu_i = 0.25 \times 10^6\ s^{-1}$, $\nu_v = 0$ (immobile vacancies), (d)–(f) concentrations are the same as (a)–(c). Red (up) and blue (down) colors correspond to interstitial and vacancy scaling function. (For interpretation of the references in color in this figure legend, the reader is referred to the web version of this article.)

Fig. 2 demonstrates clearly the time evolution of the cluster size distribution in the limiting cases of (i) *symmetrical diffusion* and (ii) *fast interstitial diffusion and reaction*. The role of defect diffusion could be well understood from a comparison of the first and second rows; both types of defects are mobile in the first row whereas only interstitials remain mobile in the second row, $v_v = 0$. As soon as diffusion of vacancies becomes slow (or immobile), single or dimer vacancy clusters start to dominate. The shape of interstitial cluster distribution stabilizes starting from the dimensionless defect concentration $C \geqslant 0.10$. The similarity of cluster distribution functions at these concentrations indicate the existence of a universal scaling function, see Fig. 2(b, c) and (e, f), respectively.

A role of defect diffusion and recombination rates is illustrated in Fig. 3 at a fixed defect concentration $C = 0.15$. The first row here shows the results for the combination of the fast interstitial diffusion and reaction limit (ii). As one can see, an increase of difference in mobilities of interstitials and vacancies leads to the increased suppression of the vacancy cluster formation, their distribution has no clear maximum, whereas single defects and dimers dominate, like in Fig. 2(d)–(f). Simultaneous increase of both recombination rate r and hoping rate v_i leads to the increase of the interstitial cluster size from $\langle s \rangle = 189$ to 371 and 655 for $v_i = r$ equal to 2, 4 and $8v_v$, respectively.

A second row in Fig. 3 demonstrates the effect of the defect recombination rate which was varied from *fast* (iii) through *normal* (i) and then the *slow* (iv) regimes (from left to the right) assuming equal mobilities of vacancies and interstitials.

In the normal diffusion limit (i) the spacial interstitial scale, ξ, remains practically constant (after a short transition region at $C < 0.05$). In cases shown in Fig. 2(a)–(c) $\xi = 18 = const$, while the characteristic cluster size, $\langle s \rangle$, increases from 29 to 62 and 99, respectively. The immobility of vacancies (Fig. 2(d)–(f)) has no effect on interstitial scale, $\xi = 18$, while it slightly increases $\langle s \rangle$ up to 32, 67 and 110, respectively.

Similarly, stability of the characteristic scale with increase of concentration can be observed in the limit of fast interstitial

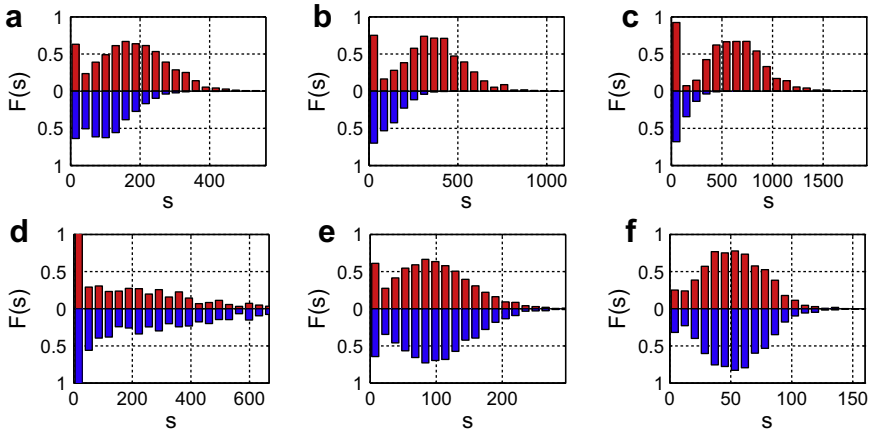

Fig. 3. Cluster distribution dependence on hoping (diffusion) and annihilation reaction rates at a fixed defect concentration, $C = 0.15$. First row (fast interstitial diffusion and reaction (ii)), $v_i = r$, both are equal to: (a) $2v_v$, (b) $4v_v$ and (c) $8v_v$. Second row (fast (iii), normal (i) and slow reaction (iv)) corresponds to the equal interstitial and vacancy hoping rates, $v_i = v_v$, with the following reaction rate variation: (d) $r = 10v_i$, (e) $r = v_i$ and (f) $r = 0.1v_i$, respectively. Red (up) and blue (down) colors correspond to interstitial and vacancy scaling function. (For interpretation of the references in color in this figure legend, the reader is referred to the web version of this article.)

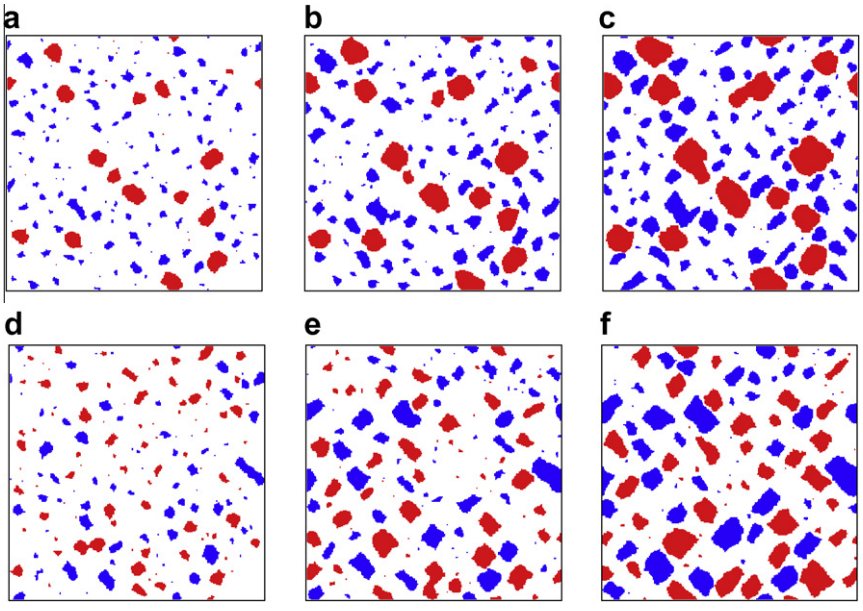

Fig. 4. Snapshots of kMC simulations at concentrations. First row, fast diffusion and reaction limit (ii) $r = v_i = 8v_v$, concentrations C: (a) 0.05, (b) 0.10 and (c) 0.15. Second row, fast reaction limit (iii) $r = 10v_i = 10v_v$, (d)–(f) concentrations are the same as (a)–(c). Interstitials are red and vacancies are blue. (For interpretation of the references in color in this figure legend, the reader is referred to the web version of this article.)

diffusion and reaction (ii). For example, for Fig. 3(c) case, we detected $\xi = 47$ and $\langle s \rangle = 643$ at concentration $C = 0.15$. For smaller concentrations $C = 0.05$ and 0.15, we found $\xi = 44$, $\langle s \rangle = 196$ and $\xi = 46$, $\langle s \rangle = 421$, respectively. This behavior indicates, that in both normal diffusion (i) and fast interstitial and reaction limits (ii) the distance between clusters remains constant despite the permanent defect production since all newly created defects become attached to pre-existing clusters (Fig. 4(a)–(c)). The clusters are weakly mobile and their growth leads to a coalescence at high concentration limit.

In this regime for different fast interstitial diffusion and reaction limits (ii) one can observe the existence of scaling in defect cluster distribution function, see Fig. 3 (first row). Despite the fact, that spacial scale is different $\xi = 25$, 35 and 47 for Fig. 3(a)–(c) cases, the distribution function shows similarity at different scales.

In turn, in the fast reaction limit (iii) the mean distance between clusters increases steadily with the defect production (Fig. 4(d)–(f)) where $\xi = 21$, 24 and 27, for concentrations $C = 0.05$, 0.10 and 0.15, respectively.

An effective defect recombination reaction eliminates small clusters. In this regime *all* cluster sizes are present, even at high concentration $C = 0.15$ (Fig. 3(d)). In the fast reaction, $r = 10 v_i$, case (iii) (when $v_i = v_v$) there is no dominating size in the cluster distribution (Fig. 3(d)).

A slow reaction rate r limit (iv) shows the behavior similar to both the normal (i) and fast interstitial diffusion and reaction limits (ii). The spatial scale establishes during initial defect accumulation stage, $C < 0.05$, and further aggregate grows is dominated by the newly created defect attachment to the pre-existing clusters.

The important conclusion is that the fast reaction (iii) both suppresses formation of a characteristic defect cluster size in the limit of equal hopping rates $v_v = v_i$ and increases cluster mobility. Small clusters dominate here, whereas large clusters are formed in the symmetrical case (ii) and then become smaller at slow reaction (iv). In the latter case cluster mobility is suppressed since it depends directly on the recombination rate.

It is interesting to compare radiation doses $G = pt$, where t is simulation time necessary to reach the concentration $C = 0.15$ in Fig. 3. In the fast (iii), normal (i) and slow (iv) reaction limits the dose is proportional to recombination rate, $G = 21.7$, 2.2 and 0.3 dpa for $r = 10$, 1 and $0.1 v_i$, respectively.

In the fast interstitial diffusion and reaction limit (ii) when $r = v_i$ and both are increased by 2, 4 and $8 v_v$, the required doses G are 3.7, 5.8 and 8.9, respectively. In its turn, the non-linear increase of G with r indicates that an increase of interstitial diffusion effectively decrease the recombination reactions. This is achieved by a creation of larger interstitial clusters, which effectively screen interstitials and thus decrease the defect recombination.

4. Conclusions

In this paper, we presented theoretical results for the kinetics of radiation defect clustering in insulating CaF_2 which is widely used in deep-UV windows and thin film optical coating. It should be noticed that the electron beam-induced radiation defects in this type of materials strongly differ from those in metals. First of all, the defects are created complementary in Frenkel pairs, rather in cascades; second, defects here possess 3D random walks rather 1D crowdion motion. Thus a *scenario* of the void formation and ordering in CaF_2 could differ considerably from that in metals (despite certain similarities). Dislocation density in insulators is much smaller than that in metals and they do not serve as efficient sinks of mobile defects (especially interstitials) as in metals.

In the kMC simulations of the radiation defect clustering we focused on the first stage of the superlattice formation what is generally believed is a random distribution of small defect clusters. However, as we have demonstrated here, the defect cluster structure is characterized by the short- and intermediate order (similar to disordered solids) while long-range order (superlattice) arises at the next step. We paid here a considerable attention to the size and space distribution functions of the defect clusters. We have demonstrated also that a non-trivial effect of the retaining a nearly constant number of the vacancy and interstitial clusters under intensive irradiation and suppressed cluster coalescence occurs only under *certain combination* of defect migration and recombination rates. In particular, too fast recombination rate of vacancies and interstitials prevents formation of large stable clusters whereas the combination of fast reaction with fast interstitial diffusion supports this process. The latter regime demonstrates the growth of large uniform-size mobile clusters which is a necessary precondition for the further void superlattice formation.

It should be also stressed that in present kMC modeling we neglected long-range (e.g. elastic) defect interactions which could be responsible for the void ordering and final superlattice formation at the second stage of the irradiation process. This study is in progress.

Acknowledgments

This research was partly supported by US DOE Basic Energy Sciences with grant DE-FG02-02ER46005. Both P.M. and G.Z. were also supported by ESF grant 2009/0202/1DP/1.1.1.2.0/09/APIA/VIAA/141.

References

[1] W. Jaeger, H. Trinkaus, J. Nucl. Mater. 205 (1993) 394.
[2] A.M. Stoneham, Rep. Prog. Phys. 70 (2007) 1055.
[3] H.C. Yu, W. Lu, Acta Mater. 53 (2005) 1799.
[4] T.H. Ding, S. Zu, L.M. Wang, Mater. Res. Soc. Symp. 849 (2005) K8.9.1–K8.9.8.
[5] T.H. Ding, L.M. Wang, et al., in press.
[6] J.G. Amar, F. Family, Phys. Rev. Lett. 74 (1995) 2066.
[7] V.N. Kuzovkov, G. Zvejnieks, E.A. Kotomin, K.D. Li, L.M. Wang, 2009. arXiv:0901.3636v1.
[8] G. Zvejnieks, V.N. Kuzovkov, Phys. Rev. E 63 (2001) 051104.
[9] http://www.balticgrid.org/.